

DMFT study on the electron-hole asymmetry of the electron correlation strength in the high T_c cuprates

Ryota Mizuno*, Masayuki Ochi, Kazuhiko Kuroki

Department of Physics, Osaka University, 1-1 Machikaneyama, Toyonaka, Osaka 560-0043, Japan

Recent experiments revealed a striking asymmetry in the phase diagram of the high temperature cuprate superconductors. The correlation effect seems strong in the hole-doped systems and weak in the electron-doped systems. On the other hand, a recent theoretical study shows that the interaction strengths (the Hubbard U) are comparable in these systems. Therefore, it is difficult to explain this asymmetry by their interaction strengths. Given this background, we analyze the one-particle spectrum of a single band model of a cuprate superconductor near the Fermi level using the dynamical mean field theory. We find the difference in the “visibility” of the strong correlation effect between the hole- and electron-doped systems. This can explain the electron-hole asymmetry of the correlation strength without introducing the difference in the interaction strength.

1. Introduction

Over thirty years have passed since the high temperature cuprate superconductors were discovered in 1986. Despite a huge number of studies, there still remain various unsolved problems in the study of this family of unconventional superconductors. The remarkable difference in the phase diagram of the cuprates between hole- and electron-doped materials is one of these unsolved issues. The mother compounds of the high temperature cuprate superconductors are usually insulating, and doping carriers, holes or electrons, induces superconductivity. It has been believed that the mother compounds of cuprates are Mott insulators due to their strong electron correlation. However, recent experimental studies have shown that, in the electron-doped systems, the electron correlation strength is not so strong that even very lightly doped samples exhibit superconductivity if they are properly annealed and the antiferromagnetism is suppressed. Some of these studies suggest that superconductivity persists even with no electron doping,¹⁻³⁾ while others show presence of antiferromagnetic long range order in the lightly doped regime,^{4,5)} so that the issue is still controversial. It was also shown experimentally that the “pseudo gap”,⁶⁻¹⁰⁾ a prominent feature of the cuprates, disappears if the antiferromagnetism is suppressed.¹¹⁾ This is consistent with a theoretical study, which shows that the pseudo gap in the electron-doped case originates from the antiferromagnetism.¹²⁾ By contrast, in the hole-doped systems, the pseudo gap exists even in the doping regime far away from the antiferromagnetic phase. Therefore, the formation mechanism of the pseudo gap in the hole-doped systems appears to be different from that in the electron-doped systems. A plausible explanation for the appearance of the pseudo gap in the hole-doped materials is the Mott insulating state, or the Mottness, of their mother compounds.¹³⁾

The above mentioned electron-hole asymmetry of the cuprates is summarized in the phase diagram shown in

Fig. 1. There is a theoretical calculation that explains the asymmetry of the superconducting phase (dome-shaped vs. monotonic) by treating the O- $2p$ orbitals properly.¹⁴⁾ On the other hand, the electron-hole asymmetry of the presence/absence of the pseudo gap phase is still an open question. It is important to note that this asymmetry occurs in a rather *abrupt* manner, i.e., there is a large difference between the hole and the electron underdoped regimes. Since the origin of the pseudo gap in the hole-doped regime is most likely to be the strong electron correlation, one may consider that the origin of this asymmetry lies in the difference in the effective electron-electron interaction strength between the hole- and electron-doped materials.¹⁵⁾ In fact, the electron-doped cuprates have been considered to exhibit weak correlation compared to a hole-doped cuprate La_2CuO_4 due to the small Cu $3d$ -O $2p$ level offset. A material with a small d - p offset has small on-site Hubbard U when mapped to an effective single band model. The difference in the d - p offset and hence the on-site U rises because the electron-doped cuprates, with the T'-type structure, have no apical oxygen, while La_2CuO_4 having the T-type structure has apical oxygens at close distance to the copper atom.¹⁶⁻¹⁹⁾ However, a recent first principles estimation²⁰⁾ has revealed that La_2CuO_4 is actually an exception that has very large d - p level offset, while many of the hole-doped cuprates have d - p offset values and hence the on-site U comparable to those in the T'-type electron doped systems. A typical example with a moderate d - p offset and U is $\text{HgBa}_2\text{CuO}_4$, in which T_c is very high ($\sim 100\text{K}$) and a pseudo gap is observed.⁹⁾ Therefore, it is difficult to explain the electron-hole asymmetry in the diagram by their interaction strength.

Given this background, we analyze the one-particle spectrum of a single band model of a cuprate superconductor near the Fermi level using dynamical mean field theory (DMFT)²¹⁾ with two kinds of impurity solvers: iterated perturbation theory (IPT)²²⁻²⁹⁾ and continuous time quantum Monte Carlo (CT-QMC)³⁰⁻³⁵⁾ methods. We adopt a model Hamiltonian derived from the first

*mizuno@presto.phys.sci.osaka-u.ac.jp

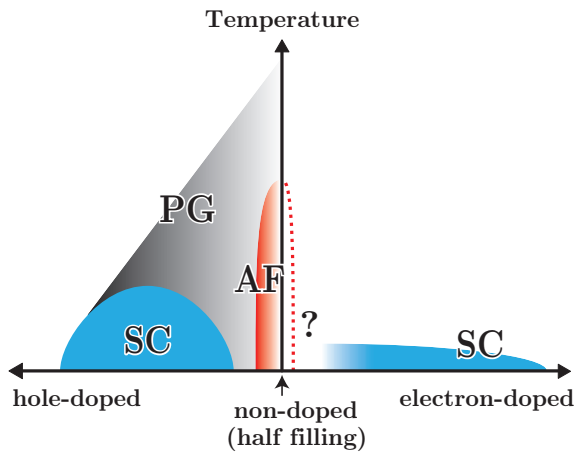


Fig. 1. (Color online) A schematic phase diagram of the high temperature cuprate superconductors: The pseudo gap exists widely over the antiferromagnetic phase and the dome-shaped superconducting phase in the hole-doped side, while T_c of the superconducting phase varies monotonically in the electron-doped side. The realization of superconductivity or antiferromagnetism in the mother compound, or in the very vicinity of it, is still controversial, especially for the electron-doped-type materials.

principles band calculation of $\text{HgBa}_2\text{CuO}_4$ since the realistic shape of the density of states (DOS) is important in the present analysis. We use the same model for both the electron and hole doped cases (just vary the electron density), since the band structure of Nd_2CuO_4 is very similar to that of $\text{HgBa}_2\text{CuO}_4$.¹⁴⁾

We find that the electron-hole asymmetry can exist even under common interaction strengths between the hole- and the electron-doped systems. The asymmetry of the spectrum already exists in the non-interacting case, but it is drastically enhanced, especially when the interaction is strong enough to make the non-doped case a Mott insulator.

This paper is organized as follows. In Sec.2, we describe the outlines of DMFT and the solvers. Computational details and results are given in Sec.3. The conclusion is given in Sec.4.

2. Method

2.1 Dynamical Mean Field Theory

We investigate the one-band Hubbard model

$$H = - \sum_{ij\sigma} t_{ij} c_{i\sigma}^\dagger c_{j\sigma} - \mu \sum_{i\sigma} c_{i\sigma}^\dagger c_{i\sigma} + U \sum_i n_{i\uparrow} n_{i\downarrow}, \quad (1)$$

where t_{ij} is the hopping matrix between sites i and j , μ and U are the chemical potential and the Coulomb repulsion, respectively. $c_{i\sigma}^{(\dagger)}$ is the annihilation (creation) operator for an electron of spin σ on site i , and $n_{i\sigma} = c_{i\sigma}^\dagger c_{i\sigma}$ is the number operator.

If the wave number dependence of the self energy is neglected, the Dyson equation for the local Green's function in the Hubbard model is equivalent to that of the impurity Green's function in the Anderson model. Therefore, in the dynamical mean field theory, the lattice problem is reduced to solving the impurity model embedded in an effective bath. This effective bath is determined by the

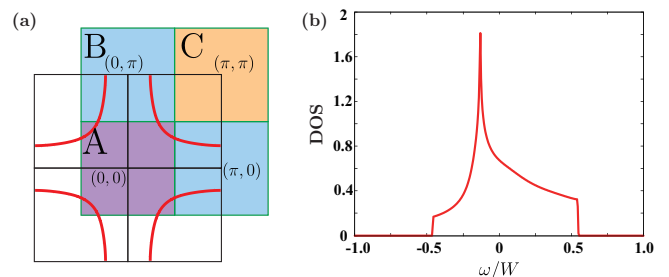


Fig. 2. (Color online) (a) Brillouin zone partitioning : The three inequivalent sectors A, B, and C are described with colors violet, cyan, and yellow, respectively. The non-interacting Fermi surface of the single-band model of $\text{HgBa}_2\text{CuO}_4$ at half filling is indicated by the red line. (b) The non-interacting density of states of $\text{HgBa}_2\text{CuO}_4$ at half filling

condition

$$\Delta(i\omega_n) = i\omega_n + \mu - \Sigma(i\omega_n) - \left[\sum_{\mathbf{k}} \frac{1}{i\omega_n + \mu - \epsilon_{\mathbf{k}} - \Sigma(i\omega_n)} \right]^{-1}, \quad (2)$$

where ω_n and \mathbf{k} are the Fermionic Matsubara frequency and the wave number, respectively. $\Delta(i\omega_n)$ is the bath hybridization function in the Anderson model, and $\epsilon_{\mathbf{k}}$ is the band dispersion in the Hubbard model. $\Sigma(i\omega_n)$ is the self energy common to both models.

In the actual calculation, one can solve the problem in the following steps : (i) Determine the initial self energy as $\Sigma(i\omega_n) = 0$. (ii) Calculate the hybridization function $\Delta(i\omega_n)$ by Eq. (2). (iii) Solve the impurity problem using $\Delta(i\omega_n)$ and obtain the new self energy. (iv) Back to step (ii). If this self-consistent loop is converged, the Green's function in the lattice problem is evaluated as

$$G_{\mathbf{k}}(i\omega_n) = \frac{1}{i\omega_n + \mu - \epsilon_{\mathbf{k}} - \Sigma(i\omega_n)}. \quad (3)$$

As mentioned above, in DMFT, the self energy has no \mathbf{k} dependence. One of the extended theories of DMFT to take the \mathbf{k} dependence into account is the dynamical cluster approximation (DCA).³⁶⁾ In this theory, \mathbf{k} dependence of the self energy is partially taken into account by dividing the Brillouin Zone into several sectors. In this study, we use both the single-site (non-extended) DMFT and the DCA. In DCA, we divide the Brillouin Zone into four sectors as shown in FIG. 2(a).

2.2 Impurity Solvers

To solve the impurity problem, various numerical methods have been proposed: iterated perturbation theory, continuous time quantum Monte Carlo, exact diagonalization (ED),³⁷⁾ non-crossing approximation (NCA),³⁸⁻⁴¹⁾ numerical renormalization group (NRG),⁴²⁾ etc. In the following section, we briefly describe IPT and CT-QMC, which we used in this study.

2.2.1 Iterated perturbation Theory

In the iterated perturbation theory,²²⁻²⁶⁾ one can solve the impurity problem by the second order perturbation theory. In the electron-hole symmetric case, it is known that IPT provides a good result⁴³⁻⁴⁵⁾ and reproduces the

exact solution in both weak and strong correlation limits.²⁸⁾ In other cases, however, the results are not so good. To overcome this weakness, the extended version of IPT for arbitrary filling²⁷⁻²⁹⁾ was proposed. In this section, we present the formalism of the extended version of IPT that we used in our study.

The self energy is parametrized by

$$\Sigma(i\omega_n) = Un + \frac{A\Sigma^{(2)}(i\omega_n)}{1 - B\Sigma^{(2)}(i\omega_n)} \quad (4)$$

where

$$\Sigma^{(2)}(i\omega_n) = U^2 T \sum_m G_0(i\omega_n + i\nu_m) \chi_0(i\nu_m) \quad (5)$$

$$\chi_0(i\nu_m) = -T \sum_l G_0(i\omega_l) G_0(i\omega_l + i\nu_m) \quad (6)$$

with the zeroth order Green's function

$$G_0(i\omega_n) = \frac{1}{i\omega_n + \mu_0 - \Delta(i\omega_n)} \quad (7)$$

and μ_0 and ν_m are the pseudo chemical potential and Bosonic Matsubara frequency, respectively. The local Green's function in the lattice problem is

$$G(i\omega_n) = \sum_{\mathbf{k}} G_{\mathbf{k}}(i\omega_n) = \sum_{\mathbf{k}} \frac{1}{i\omega_n + \mu - \epsilon_{\mathbf{k}} - \Sigma(i\omega_n)}. \quad (8)$$

The constants A and B are determined such that one reproduces the exact solution in the high frequency and the atomic limits:

$$A = \frac{n(1-n)}{n_0(1-n_0)}, \quad B = \frac{\mu_0 - \mu + (1-n)U}{n_0(1-n_0)U^2}, \quad (9)$$

where n_0 and n are the electron numbers evaluated from $G_0(i\omega_n)$ and $G(i\omega_n)$, respectively.

The chemical potential μ is determined by fixing n at the input value, while μ_0 is still a free parameter. Among the various suggested conditions for determining μ_0 ,^{28,29,46,47)} here we employ the condition $n = n_0$. In this condition, the IPT calculation provides a qualitatively good result except in the case when the Coulomb interaction strength is too large.^{28,29)}

2.2.2 Continuous Time Quantum Monte Carlo Method

Continuous time quantum Monte Carlo method is numerically exact. Among the several algorithms of CT-QMC, here we adopt CT-INT in this study. This algorithm, developed by Rubtsov *et al.*,^{31,32)} is based on the Monte Carlo summation of all diagrams obtained from the expansion of the partition function in powers of the interaction U . We describe only a brief outline of CT-INT in this section. For efficient computation, we also employ the submatrix update algorithm^{34,35)} extended to CT-INT.³³⁾

We divide the impurity Hamiltonian into two parts, $H = H_0 + H_i$. H_i is the interacting term including U . The partition function is

$$Z = \text{Tr} \left[e^{-\beta H_0} T_\tau \exp \left(- \int_0^\beta d\tau H_i(\tau) \right) \right], \quad (10)$$

where $A(\tau) = e^{\tau H_0} A e^{-\tau H_0}$ is the interaction representation of the operator A , and T_τ is the time ordering operator for the imaginary time. The statistical average for H_0 is

$$\langle A \rangle_0 = \frac{1}{Z_0} \text{Tr} [e^{-\beta H_0} A], \quad Z_0 = \text{Tr} e^{-\beta H_0}. \quad (11)$$

We expand the partition function in powers of H_i and obtain

$$\frac{Z}{Z_0} = \sum_{n=0}^{\infty} \int_0^\beta d\tau_n \cdots d\tau_2 d\tau_1 \times (-1)^n \langle T_\tau H_i(\tau_n) \cdots H_i(\tau_2) H_i(\tau_1) \rangle_0. \quad (12)$$

The statistical average of the operator A for the full Hamiltonian H is described as

$$\langle A \rangle = \frac{\sum_n \int_n d\tau \langle \hat{P}(q_n) A(q_n) \rangle_0}{\sum_n \int_n d\tau P(q_n)}, \quad (13)$$

where

$$P(q_n) = \langle \hat{P}(q_n) \rangle_0 = (-1)^n \langle T_\tau H_i(\tau_n) \cdots H_i(\tau_2) H_i(\tau_1) \rangle_0 \quad (14)$$

$$q_n = \{\tau_1, \tau_2, \cdots, \tau_n\} \quad (15)$$

$$\int_n d\tau = \frac{1}{n!} \int_0^\beta d\tau_n \cdots d\tau_2 d\tau_1. \quad (16)$$

In the Monte Carlo method, the Markov chain of the imaginary time arrangement q_n that follows the probability distribution $P(q_n)$ is generated. The statistical average of A is estimated as

$$\langle A \rangle = \frac{\sum_n \int_n d\tau P(q_n) \frac{\langle \hat{P}(q_n) A(q_n) \rangle_0}{P(q_n)}}{\sum_n \int_n d\tau P(q_n)} \simeq \frac{1}{N_s} \sum_{\{q_n\}} \frac{\langle \hat{P}(q_n) A(q_n) \rangle_0}{P(q_n)} \quad (17)$$

We can use the Wick's theorem since H_0 has a quadratic form in terms of the creation and annihilation operators of electrons. Then we obtain

$$P(q_n) = (-U)^n \prod_{\sigma} \det \mathcal{G}_{\sigma}, \quad (18)$$

where $(\mathcal{G}_{\sigma})_{ij} = \mathcal{G}_{\sigma}(\tau_i - \tau_j)$ is the zeroth order Green's function in the impurity model.

3. Results

To see the electron-hole asymmetry of the correlation strength, we analyze the filling dependence of the quantity $\beta G_{\mathbf{k}}(\beta/2)$ ⁴⁸⁻⁵⁰⁾ defined as

$$\beta G_{\mathbf{k}}(\beta/2) = \frac{1}{2\pi T} \int_{-\infty}^{\infty} \frac{A_{\mathbf{k}}(\omega) d\omega}{\cosh(\omega/2T)}, \quad (19)$$

where $A_{\mathbf{k}}(\omega) = -\frac{1}{\pi} \text{Im} G_{\mathbf{k}}(\omega)$ is the spectrum function. Namely, $\beta G_{\mathbf{k}}(\beta/2)$ represents the number of states near the Fermi level. In the rest of this paper, we sometimes describe this quantity as βG for simplicity.

3.1 Computational Details

First, we obtain the band structure of $\text{HgBa}_2\text{CuO}_4$ by performing the first principle calculation using the WIEN2k package.⁵¹⁾ We derive the model Hamiltonian based on the first principles calculation since the realistic shape of the density of states is essential to the present analysis. We employ the density functional theory (DFT) using the generalized gradient approximation.⁵²⁾ From this band structure, we obtain a single-orbital model corresponding to $\text{Cu } d_{x^2-y^2}$ with a maximally localized Wannier basis.^{53,54)} Figure.2(b) shows the Fermi surface and the density of states of this model at half filling. Since the electronic structure of the electron-doped Nd_2CuO_4 is very similar to that of $\text{HgBa}_2\text{CuO}_4$,¹⁴⁾ we adopt this model not only in the hole doped regime, but also in the electron-doped regime. We take into account using DMFT the electron correlation effect beyond DFT. We take the following two approaches in the DMFT calculation. One is the DCA calculation with the CT-QMC solver. This approach enables us to obtain the \mathbf{k} dependence of the self energy, and to analyze the pseudo gap directly, although its numerical cost is rather large. The other is the single-site DMFT calculation with the IPT solver. This enables us to analyze a wide range of parameters (the band filling n , the temperature T , the interaction strength U) due to its very low numerical cost, although \mathbf{k} dependence of the self energy is neglected. In the DCA with CT-QMC, we restrict the band filling to the range $0.7 \leq n \leq 1.2$, and fix the temperature at $T/W = 0.005$, and the interaction strength at $U/W = 1.0$ (W is the band width). The band filling range considered here corresponds to the doping concentration where the pseudo gap is observed experimentally. In the single-site DMFT with IPT, the calculation is performed in the band filling range $0.2 \leq n \leq 1.7$ with several values of T and U , namely $T/W = 0.05, 0.025, 0.01, 0.005, 0.0025, 0.00125$ and $U/W = 0.005, 1.0, 1.5$. Our intention for hypothetically taking different values of U in the single-site DMFT is to see how the electron-hole asymmetry of the electron correlation emerges with and without the Mottness, while assuming the same value of U regardless of the (electron or hole) doping. We should also note that the single-site DMFT underestimates the tendency toward Mott transition compared to DCA, so that, roughly speaking, $U/W = 1.5$ in the single-site DMFT can be considered as corresponding to $U/W = 1.0$ in DCA.

3.2 \mathbf{k} Dependence of βG by the DCA

As mentioned in Sec.2.1, in the DCA calculation, we divide the Brillouin zone into four sectors as shown in FIG. 2(a). βG in sector X ($X = \text{A, B, C}$) is defined as

$$\beta G_X(\beta/2) = \frac{1}{N_c} \sum_{\mathbf{k} \in X} \beta G_{\mathbf{k}}(\beta/2), \quad (20)$$

where N_c is the number of \mathbf{k} points in the sector. Figure. 3 (a) shows βG_X (solid line) and $\beta G_X^{U=0}$ (dashed line) in $0.7 < n < 1.2$, where $\beta G_X^{U=0}$ represents the non-interacting βG_X , and (b) shows the ratio $\beta G_X/\beta G_X^{U=0}$ in the underdoped regime $0.9 < n < 1.1$. One can see

that there is a large difference between the hole- and electron-doped sides. The most important point is the electron-hole asymmetry of βG_B (blue line in FIG. 3). βG_B is almost equal to $\beta G_B^{U=0}$ at $n = 0.7$ and approaches 0 as n approaches 1, but as soon as n exceeds 1, βG_B suddenly recovers to about 50% value of $\beta G_B^{U=0}$. Namely, in the underdoped regime, the correlation effect emerges strongly in the hole-doped side and weakly in the electron-doped side. This tendency was shown in a previous work,⁴⁸⁾ but there βG was plotted as a function of the chemical potential, whereas it is plotted against the electron density here, so that it can be seen more clearly that the electron-hole asymmetry is prominent in the underdoped regime.

As for βG_A (violet line in FIG. 3), we also observe an electron-hole asymmetry; in the electron-doped side in particular, βG_A is almost zero. This, however, should not be taken as an indication of the strong correlation effect as in sector B of the hole-doped case. In fact, it is known that the antinodal regime of the Fermi surface is strongly affected by the spin fluctuation caused by the (π, π) nesting, a weak coupling effect, when electrons are doped.⁵⁵⁾ The 2×2 partitioning of the Brillouin zone adopted in the present study overestimates this effect because the only portion of the Fermi surface included in sector A is the very vicinity of the antinodal point. The overestimation can indeed be confirmed by looking into the results in Ref.[48], where the Brillouin zone was divided into eight sectors. There, the electron-hole asymmetry of the antinodal sector is barely seen.

3.3 T Dependence of βG by the Single-site DMFT

We calculate the following average value of $\beta G_{\mathbf{k}}$ in the Brillouin zone since the self energy is independent of \mathbf{k} in the single-site DMFT:

$$\beta G(\beta/2) = \frac{1}{N} \sum_{\mathbf{k} \in \text{BZ}} \beta G_{\mathbf{k}}(\beta/2), \quad (21)$$

where N is the number of \mathbf{k} points in the Brillouin zone. In FIG. 4(a)-(c), βG is plotted against the band filling n for three values of U and various temperatures. When U is nearly zero, the temperature dependence of βG is barely seen except in the band filling regime where the Fermi level sits close to the van Hove singularity point. When U is increased to an intermediate value where the Mott transition still does not take place at $n = 1$, the band filling range where the temperature dependence is present is broadened, although the band filling dependence is continuous in this case. A more interesting electron-hole asymmetry is seen in the underdoped regime when U is further increased so that the Mott transition occurs at $n = 1$. Namely, the temperature dependence is barely present in the electron-doped regime ($n > 1.1$) when the temperature is low, as if the electron correlation effect is absent, while a strong temperature dependence is seen in the hole-doped side.⁵⁶⁾ Hence, the electron-hole asymmetry occurs discontinuously with respect to the band filling in the presence of the Mottness. In other words, the ‘‘visibility’’ of the electron correlation effect changes abruptly between the hole and the

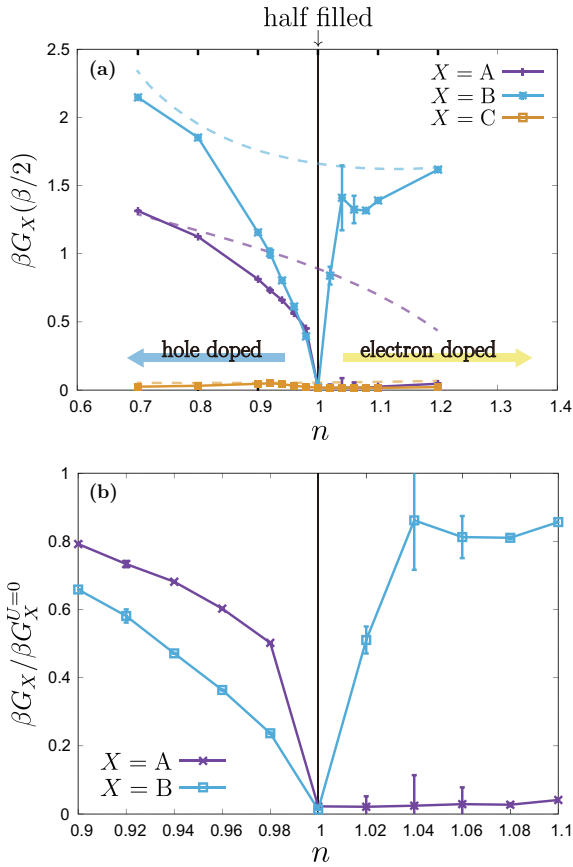


Fig. 3. (Color online) (a) The violet, blue, and orange lines indicate βG_X defined with Eq. (20) of sectors A, B, and C, respectively. The dashed lines indicate βG_X in the non-interacting case. (b) The violet and blue lines indicate the ratios $\beta G_X / \beta G_X^{U=0}$ of sectors A and B, respectively. The temperature and interaction strength are $T/W = 0.005$ and $U/W = 1.0$.

electron-doped cases.

In order to understand the origin of this electron-hole asymmetry, we investigate the spectrum function $A(\omega) = -\frac{1}{\pi} \text{Im}G(\omega)$ obtained by performing the analytical continuation with Padé approximation.⁵⁷⁾ The enlarged view of the spectrum near the Fermi level at $T/W = 0.005$ is shown in FIG. 5. The orange band describes the temperature range for which the integration in βG is effective. In the case of $U/W = 1.0$ shown in FIG. 5(a) (the Mottness is absent), the peak of the spectrum is located in the range $\omega < 0$ reflecting the shape of the non-interacting DOS shown in FIG. 2(b) that has the van Hove singularity in $\omega < 0$. The spectrum moves continuously when the band filling is varied, which leads to the continuous band filling variance of the temperature dependence of βG seen in Fig. 4(b). The peak of the spectrum in the hole-doped side described by the blue tone colors is closer to the Fermi level than that in the electron-doped side described by the yellow tone colors, so that a larger temperature dependence exists in the hole-doped side. By contrast, in the case of $U/W = 1.5$ shown in FIG. 5(b) (the Mottness is present), the variation of the spectrum with respect to the band filling is qualitatively different from that in $U/W = 1.0$. The peak of the spectrum in the hole-doped

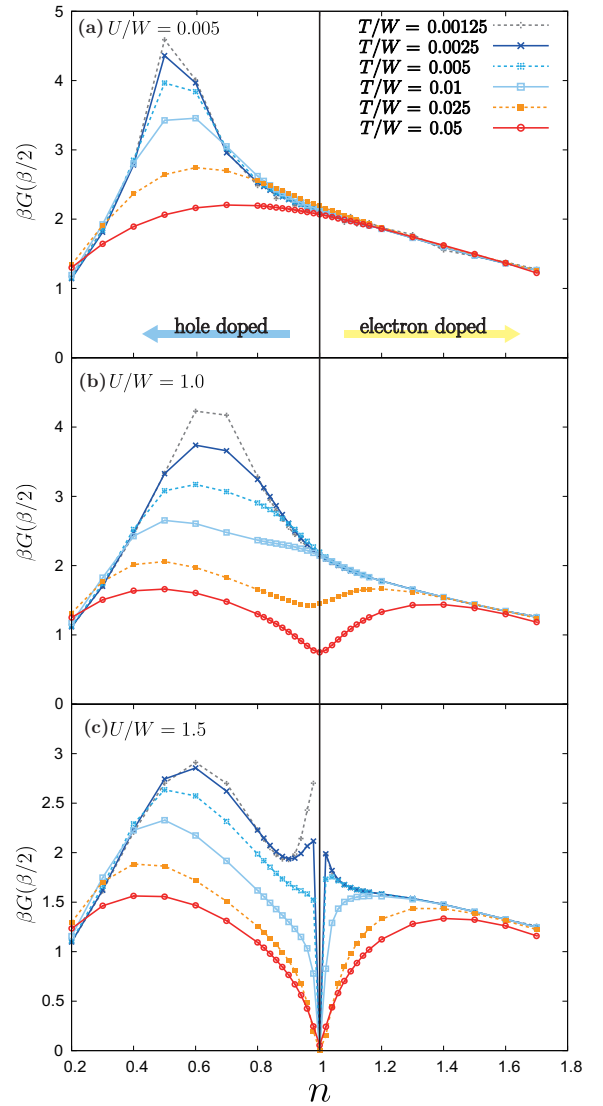


Fig. 4. (Color online) βG defined with Eqs. (21) are plotted against the band filling n for $U/W =$ (a) 0.005, (b) 1.0, and (c) 1.5 with various temperatures.

side is located within the integration temperature range and barely moves when the band filling is varied, while the situation in the electron-doped side is similar to that in the case $U/W = 1.0$. This discontinuous behavior of the spectrum gives rise to the discontinuous temperature dependence shown in FIG. 4(c).

4. Conclusion

In conclusion, we have shown that the electron-hole asymmetry of the electron correlation effect can exist even under common interaction strengths and the band structure between the hole- and electron-doped systems. The presence of this electron-hole asymmetry itself is not so surprising because the non-interacting DOS is already asymmetric. However, the asymmetric feature of the DOS alone cannot account for the striking asymmetry observed in the experiments. Our important finding is that considering the strong correlation effect in addition to the asymmetry of the DOS makes it possible to understand the experimental observation. To be more precise, assuming that the mother compounds of both the electron-doped and the hole-doped cuprates are Mott in-

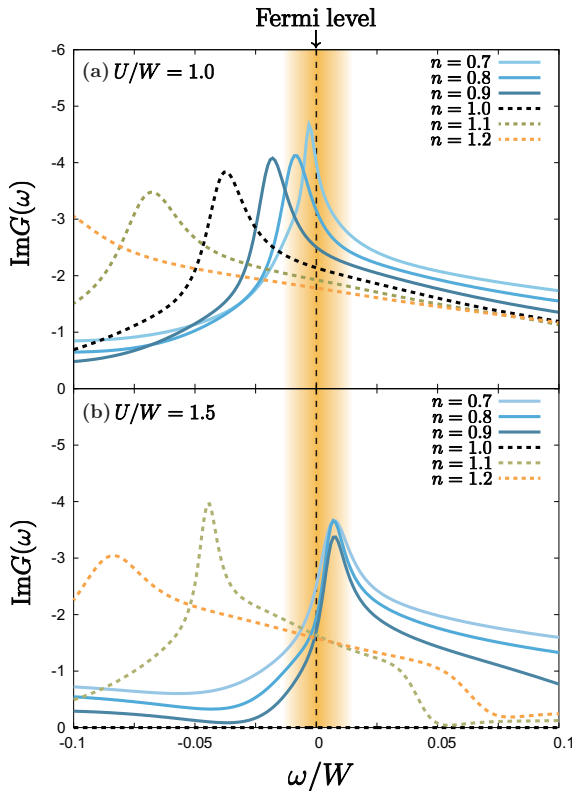


Fig. 5. (Color online) The spectrum near the Fermi level: The curves with blue tone colors describe the spectrum in the hole-doped side and with yellow tone colors in the electron-doped side. The black curve describes the spectrum of $n = 1$, which vanishes in the lower panel due to the Mottness. The orange band describes the temperature range for which the integration in βG is effective. The temperature is $T/W = 0.005$.

sulators, the combination of the Mottness and the asymmetry of the DOS can explain the discontinuous electron-hole asymmetry in the phase diagram of the cuprates. The fact that the present results are obtained under a common value of U between the hole and the electron-doped cases implies that the electron correlation effect is less visible in the electron-doped regime.⁵⁸⁾

In this sense, it can be said that the origin of the electron-hole asymmetry of the cuprates is the asymmetry of the “visibility” of the strong correlation effect.

5. Acknowledgements

We are grateful to Yusuke Nomura and Shiro Sakai for providing the CT-INT code, and also providing useful comments regarding the manuscript. A part of the calculations was performed using supercomputers at the Supercomputer Center, Institute of Solid State Physics, The University of Tokyo. This study was supported by Grant-in-Aid for Young Scientists (B) (No.JP15K17724), Grant-in-Aid for Scientific Research on Innovative Areas (No.JP17H05481), Grants-in-Aid for Scientific Research (A) (No.JP26247057) and Grants-in-Aid for Scientific Research (B) (No.JP16H04338) from the Japan Society for the Promotion of Science.

- 1) M. Brinkmann, T. Rex, H. Bach, and K. Westerholt: Phys. Rev. Lett. **74** (1995) 4927.
- 2) A. Tsukada, Y. Krockenberger, M. Noda, H. Yamamoto, D. Manske, L. Alf, and M. Naito: Solid State Communications **133** (2005) 427.
- 3) Y. Krockenberger, H. Irie, O. Matsumoto, K. Yamagami, M. Mitsuhashi, A. Tsukada, M. Naito, and H. Yamamoto: Scientific Reports **3** (2013) 2235.
- 4) H. Saadaoui, Z. Salman, H. Luetkens, T. Prokscha, A. Suter, W. A. MacFarlane, Y. Jiang, K. Jin, R. L. Greene, E. Morenzoni, and R. F. Kiefl: Nature Communications **6** (2015) 6041.
- 5) D. Song *et al.*⁵⁹⁾ studied the electron-doped samples $\text{Pr}_{1-x}\text{LaCe}_x\text{CuO}_{4-\delta}$ prepared by a normal annealing process, where suppression of T_c due to the antiferromagnetic short-range correlation is found in the underdoped regime.
- 6) H. Alloul, T. Ohno, and P. Mendels: Phys. Rev. Lett. **63** (1989) 1700.
- 7) W. W. Warren, R. E. Walstedt, G. F. Brennert, R. J. Cava, R. Tycko, R. F. Bell, and G. Dabbagh: Phys. Rev. Lett. **62** (1989) 1193.
- 8) M. R. Norman, H. Ding, M. Randeria, J. C. Campuzano, T. Yokoya, T. Takeuchi, T. Takahashi, T. Mochiku, K. Kadowaki, P. Guptasarma, and D. G. Hinks: Nature **392** (1998) 157.
- 9) A. Yamamoto, W.-Z. Hu, and S. Tajima: Phys. Rev. B **63** (2000) 024504.
- 10) N. P. Armitage, P. Fournier, and R. L. Greene: Rev. Mod. Phys. **82** (2010) 2421.
- 11) M. Horio, T. Adachi, Y. Mori, A. Takahashi, T. Yoshida, H. Suzuki, L. Ambolode, K. Okazaki, K. Ono, H. Kumigashira, H. Anzai, M. Arita, H. Namatame, M. Taniguchi, D. Ootsuki, K. Sawada, M. Takahashi, T. Mizokawa, Y. Koike, and A. Fujimori: Nature Communications **7** (2016) 10567.
- 12) M. M. c. v. Zemljič, P. Prelovšek, and T. Tohyama: Phys. Rev. B **76** (2007) 012502.
- 13) C. Huscroft, M. Jarrell, T. Maier, S. Moukouri, and A. N. Tahvildarzadeh: Phys. Rev. Lett. **86** (2001) 139.
- 14) D. Ogura and K. Kuroki: Phys. Rev. B **92** (2015) 144511.
- 15) H. Yokoyama, M. Ogata, Y. Tanaka, K. Kobayashi, and H. Tsuchiura: J. Phys. Soc. Jpn **82** (2013) 014707.
- 16) C. Weber, K. Haule, and G. Kotliar: Nature Physics **6** (2010) 574.
- 17) C. Weber, K. Haule, and G. Kotliar: Phys. Rev. B **82** (2010) 125107.
- 18) H. Das and T. Saha-Dasgupta: Phys. Rev. B **79** (2009) 134522.
- 19) T. Adachi, Y. Mori, A. Takahashi, M. Kato, T. Nishizaki, T. Sasaki, N. Kobayashi, and Y. Koike: J. Phys. Soc. Jpn **82** (2013) 063713.
- 20) S. W. Jang, H. Sakakibara, H. Kino, T. Kotani, K. Kuroki, and M. J. Han: Scientific Reports **6** (2016) 33397.
- 21) A. Georges, G. Kotliar, W. Krauth, and M. J. Rozenberg: Rev. Mod. Phys. **68** (1996) 13.
- 22) K. Yosida and K. Yamada: Progress of Theoretical Physics Supplement **46** (1970) 244.
- 23) K. Yamada: Progress of Theoretical Physics **53** (1975) 970.
- 24) K. Yosida and K. Yamada: Progress of Theoretical Physics **53** (1975) 1286.
- 25) K. Yamada: Progress of Theoretical Physics **54** (1975) 316.
- 26) A. Georges and G. Kotliar: Phys. Rev. B **45** (1992) 6479.
- 27) H. Kajueter and G. Kotliar: Phys. Rev. Lett. **77** (1996) 131.
- 28) M. Potthoff, T. Wegner, and W. Nolting: Phys. Rev. B **55** (1997) 16132.
- 29) L.-F. Arsenault, P. Smon, and A.-M. S. Tremblay, Phys. Rev. B **86** (2012) 085133.
- 30) E. Gull, P. Werner, A. Millis, and M. Troyer: Phys. Rev. B **76** (2007) 235123.
- 31) A. N. Rubtsov, V. V. Savkin, and A. I. Lichtenstein: Phys. Rev. B **72** (2005) 035122.
- 32) A. N. Rubtsov and A. I. Lichtenstein: Journal of Experimental and Theoretical Physics Letters **80** (2004) 61.
- 33) Y. Nomura, S. Sakai, and R. Arita: Phys. Rev. B **89** (2014) 195146.
- 34) P. K. V. V. Nukala, T. A. Maier, M. S. Summers, G. Alvarez,

- and T. C. Schulthess: Phys. Rev. B **80** (2009) 195111.
- 35) E. Gull, P. Staar, S. Fuchs, P. Nukala, M. S. Summers, T. Pruschke, T. C. Schulthess, and T. Maier: Phys. Rev. B **83** (2011) 075122.
- 36) T. Maier, M. Jarrell, T. Pruschke, and M. H. Hettler: Rev. Mod. Phys. **77** (2005) 1027.
- 37) M. Caffarel and W. Krauth: Phys. Rev. Lett. **72** (1994) 1545.
- 38) Y. Kuramoto: Zeitschrift für Physik B Condensed Matter **53** (1983) 37.
- 39) Y. Kuramoto and H. Kojima: Zeitschrift für Physik B Condensed Matter **57** (1984) 95.
- 40) H. Kojima, Y. Kuramoto, and M. Tachiki: Zeitschrift für Physik B Condensed Matter **54** (1984) 293.
- 41) Y. Kuramoto: Zeitschrift für Physik B Condensed Matter **65** (1986) 29.
- 42) R. Bulla, T. A. Costi, and T. Pruschke: Rev. Mod. Phys. **80** (2008) 395.
- 43) A. Georges and W. Krauth: Phys. Rev. B **48** (1993) 7167.
- 44) X. Y. Zhang, M. J. Rozenberg, and G. Kotliar: Phys. Rev. Lett. **70** (1993) 1666.
- 45) M. J. Rozenberg, G. Kotliar, and X. Y. Zhang: Phys. Rev. B **49** (1994) 10181.
- 46) A. Martín-Rodero, E. Louis, F. Flores, and C. Tejedor: Phys. Rev. B **33** (1986) 1814.
- 47) D. Meyer, T. Wegner, M. Potthoff, and W. Nolting: Physica B: Condensed Matter **270** (1999) 225 .
- 48) E. Gull, O. Parcollet, P. Werner, and A. J. Millis: Phys. Rev. B **80** (2009) 245102.
- 49) P. Werner, E. Gull, O. Parcollet, and A. J. Millis: Phys. Rev. B **80** (2009) 045120.
- 50) E. Gull, M. Ferrero, O. Parcollet, A. Georges, and A. J. Millis: Phys. Rev. B **82** (2010) 155101.
- 51) P. Blaha, K. Schwarz, G. K. H. Madsen, D. Kvasnicka, and J. Luitz: *WIEN2K, An Augmented Plane Wave + Local Orbitals Program for Calculating Crystal Properties* (Karlheinz Schwarz, Techn. Universität Wien, Austria, 2001).
- 52) J. P. Perdew, K. Burke, and M. Ernzerhof: Phys. Rev. Lett. **77** (1996) 3865.
- 53) J. Kuneš, R. Arita, P. Wissgott, A. Toschi, H. Ikeda, and K. Held: Computer Physics Communications **181** (2010) 1888 .
- 54) A. A. Mostofi, J. R. Yates, Y.-S. Lee, I. Souza, D. Vanderbilt, and N. Marzari: Computer Physics Communications **178** (2008) 685 .
- 55) K. Kuroki and H. Aoki: J. Phys. Soc. Jpn **67** (1998) 1533.
- 56) The tendency that electron-hole asymmetry is barely seen in the high temperature regime is consistent with a DMFT analysis given in Refs. [60, 61].
- 57) H. J. Vidberg and J. W. Serene: Journal of Low Temperature Physics **29** (1977) 179.
- 58) In Ref. [62], the superconducting T_c of the single band Hubbard model was found to be lower in the hole-doped regime than that in the electron-doped regime due to the presence of the pseudo gap, assuming the same values of the on-site Hubbard U between them. This inconsistency with the experimental observation may be resolved by adopting the three band model that explicitly considers the oxygen p orbitals¹⁴⁾ Even when the three band model is adopted, the present conclusion regarding the electron-hole asymmetry of the electron correlation strength will not be affected, since the present conclusion relies only on the asymmetric shape of the density of states.
- 59) D. Song, G. Han, W. Kyung, J. Seo, S. Cho, B. S. Kim, M. Arita, K. Shimada, H. Namatame, M. Taniguchi, Y. Yoshida, H. Eisaki, S. R. Park, and C. Kim: Phys. Rev. Lett. **118** (2017) 137001.
- 60) L. de' Medici, X. Wang, M. Capone, and A. J. Millis: Phys. Rev. B **80** (2009) 054501.
- 61) X. Wang, L. de' Medici, and A. J. Millis: Phys. Rev. B **83** (2011) 094501.
- 62) X. Chen, J. P. F. LeBlanc, and E. Gull: Phys. Rev. Lett. **115** (2015) 116402.